JOURNAL OF GEOPHYSICAL RESEARCH, VOL. 111, D23S57, doi:10.1029/2006JD007456, 2006

Trajectory model validation using newly developed altitude-controlled balloons during the International Consortium for Atmospheric Research on Transport and Transformations 2004 campaign

Emily E. Riddle,[1,2] Paul B. Voss,[3,4] Andreas Stohl,[5] Daniel Holcomb,[6] Darren Maczka,[6] K. Washburn,[7] and Robert W. Talbot[8]

Received 28 April 2006; revised 13 September 2006; accepted 20 September 2006; published 2 December 2006.

[1] During the summer of 2004, five altitude-controlled tracking balloons were flown as part of the International Consortium for Atmospheric Research on Transport and Transformations (ICARTT) campaign. These Controlled Meteorological (CMET) balloons, newly developed at the University of Massachusetts, are notable for their light weight (~1 kg mass), efficient altitude control, ease of launch, long-duration flight capability, and ability to perform repeated quasi-Lagrangian soundings. The balloons were embedded in urban plumes from New York and Boston which they tracked over New England, eastern Canada, and the Atlantic Ocean while maintaining a nearly constant altitude. The flights ranged from 10 to 111 hours and covered a maximum distance of 3000 km. Balloon flight tracks are used here to assess the accuracy of trajectory models during intensive aircraft sampling periods. A new method is presented for increasing the number of available reference trajectories by dividing the balloon flights into shorter segments for statistical analysis. For trajectory durations between 2 and 12 hours, mean trajectory errors are found to be approximately 26% and 34% of the flight distance for ECMWF-based and GFS-based trajectories, respectively. Anomalously large model errors observed during three of the flights are found to be the result of a narrow low-level jet (15 July) and synoptic-scale flow patterns (9 and 10 August). The results from this study should be useful to researchers evaluating the performance of trajectory models and chemical transport models during the ICARTT campaign. Complete CMET balloon and model trajectory data sets are available as a supplement to this paper.

Citation: Riddle, E. E., P. B. Voss, A. Stohl, D. Holcomb, D. Maczka, K. Washburn, and R. W. Talbot (2006), Trajectory model validation using newly developed altitude-controlled balloons during the International Consortium for Atmospheric Research on Transport and Transformations 2004 campaign, *J. Geophys. Res.*, *111*, D23S57, doi:10.1029/2006JD007456.

1. Introduction

[2] The ICARTT campaign brought together researchers from North America and Europe during the summer of 2004 to study the transport and chemical transformation of pollutants in the eastern United States and Canada. The intensive study sought to answer questions concerning air quality in New England, the export of North American pollutants to Europe, and the radiative effects of aerosols on regional climate. Findings from the data collected over the course of the 2-month campaign will provide information to help guide air quality regulations and improve our understanding of the aerosol forcings that influence global climate change.

[3] One priority of the campaign was to examine chemical transformations and other atmospheric processes from a Lagrangian perspective. The University of Massachusetts contributed five newly developed Controlled Meteorological (CMET) balloons toward this effort. The balloons were released between 15 July 2004 and 10 August 2004 into polluted air masses traveling up the coast from the east coast urban corridor. Figure 1 shows flight tracks from the five ICARTT flights. The five flights are identified here and in the remainder of the manuscript by their launch date (e.g., 040715 for the flight beginning on 15 July 2004).

[4] The synoptic environment during of each of the five flights is shown in Figure 2. The balloons were released into low-level outflow events following the stagnation of an air

[1]Department of Geosciences, University of Massachusetts, Amherst, Massachusetts, USA.
[2]Also at Department of Earth and Atmospheric Sciences, Cornell University, Ithaca, New York, USA.
[3]Department of Geosciences, University of Massachusetts, Amherst, Massachusetts, USA.
[4]Also at Picker Engineering Program, Smith College, Northampton, Massachusetts, USA.
[5]Norwegian Institute for Air Research, Kjeller, Norway.
[6]Department of Electrical and Computer Engineering, University of Massachusetts, Amherst, Massachusetts, USA.
[7]Department of Mechanical and Industrial Engineering, University of Massachusetts, Amherst, Massachusetts, USA.
[8]Institute for the Study of Earth, Oceans, and Space, University of New Hampshire, Durham, New Hampshire, USA.

0148-0227/06/2006JD007456$09.00

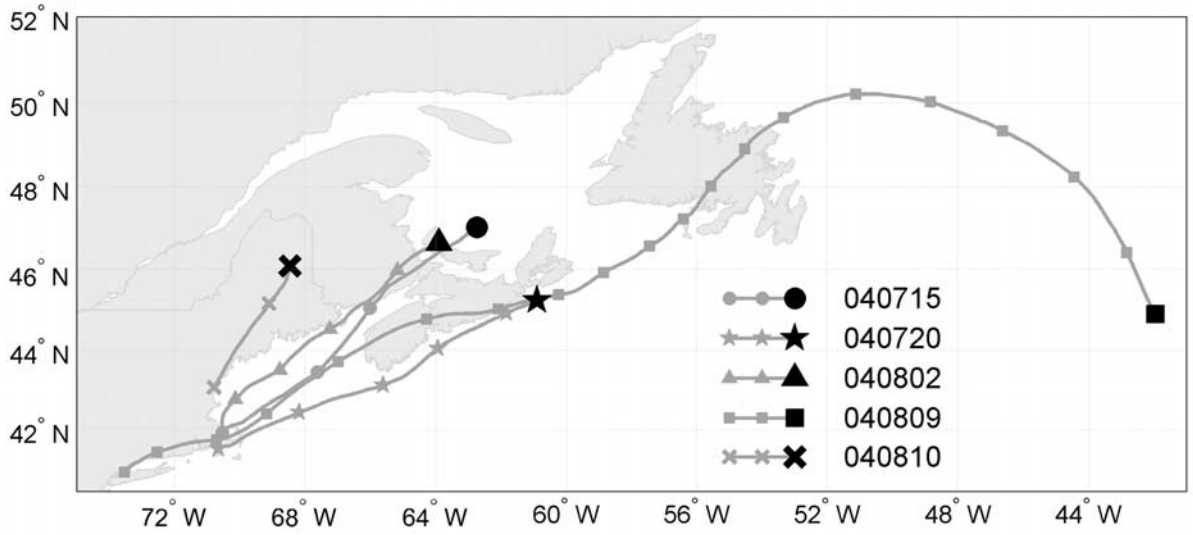

Figure 1. Flight tracks of five CMET tracking balloons released during the 2004 ICARTT campaign. Flights are referred to by their start dates (e.g., 040715 for the flight beginning on 15 July 2004). Shaded symbols are placed at 6-hour intervals along the trajectories.

mass over the northeast urban corridor. Such conditions often occurred in the warm-sector southwesterly flow preceding an approaching cold front.

[5] The balloons provided a stand-alone quasi-Lagrangian platform for meteorological and, in one case, chemical measurements and were also used as marker buoys to track air parcels as part of coordinated aircraft/balloon Lagrangian experiments. These flights follow a long history of balloon-guided Lagrangian experiments [e.g., *Meagher et al.*, 1978; *Feigley and Jeffries*, 1979; *D. W. Johnson et al.*, 2000], which have been reviewed by *Zak* [1983] and *Businger et al.* [1996].

[6] In the present paper, five CMET balloon flight tracks are used to evaluate the performance of trajectory models and chemical transport models during ICARTT sampling periods.

2. Background

[7] Trajectory models (e.g., FLEXTRA, HYSPLIT) and Lagrangian particle dispersion models (e.g., FLEXPART) were both used extensively during the course of the ICARTT campaign to predict the location of polluted air masses, plan aircraft missions, and develop Lagrangian sampling strategies. Run in ''backward mode,'' these models are also widely used in postcampaign analysis to identify the history and potential source contributions of sampled air masses and to pinpoint potential Lagrangian experiments. Since all of these model applications depend fundamentally on the accuracy of trajectory calculations, it is necessary that trajectory models are validated, particularly during interesting outflow events.

[8] Validation of trajectory models is a challenge because of the fact that real atmospheric trajectories are difficult to measure or even, in some cases, to define. Because of this, much of the literature on trajectory modeling examines the sensitivity of the models to a variety of different parameters, including (1) the source of wind field data [e.g., *Kahl et al.*, 1989; *Pickering et al.*, 1996], (2) the wind field grid resolution [e.g., *Rolph and Draxler*, 1990; *Stohl et al.*, 1995], (3) the model forecast time [e.g., *Stunder*, 1996; *Haagenson et al.*, 1990], and (4) the trajectory type (kinematic, isobaric, isosigma or isentropic) [e.g., *Stohl and Seibert*, 1998; *Draxler*, 1996]. The variation between model runs can be used to evaluate the likely range of errors resulting from the factors listed above. However, the actual overall size of the trajectory error cannot be known without physical validation data.

[9] The accuracy of a trajectory model can be determined by comparison with a ''true'' reference trajectory. Unfortunately, because of distortions due to turbulent mixing and wind shear, the meaning of a ''true'' atmospheric trajectory is not always obvious. While deferring a full discussion of this issue to section 4, we note that the reference trajectory should generally be representative of bulk transport at the smallest resolvable scale of the model.

[10] A number of different atmospheric tracers have been used for reference trajectories, each with its own challenges. The four most important of these are natural material tracers [e.g., *Reiff et al.*, 1986; *McQueen and Draxler*, 1994], intentionally released chemical tracers [e.g., *Haagenson et al.*, 1987, 1990; *Draxler*, 1987, 1991], dynamical tracers [e.g., *Stohl and Seibert*, 1998] and drifting balloons [e.g., *Clarke et al.*, 1983; *Knudsen and Carver*, 1994; *Draxler*, 1996; *Baumann and Stohl*, 1997; *Stohl and Koffi*, 1998]. These studies report errors between 2 and 30% of the total trajectory length for trajectories between several hours and several days in duration. A comprehensive review of trajectory model validation and sensitivity studies is provided by *Stohl* [1998].

[11] Drifting balloons provide a valuable tool for validating trajectory models because they follow horizontal air motion very accurately and can be more easily tracked than other types of tracers. However, there are also limitations to using balloons as a validation tool. A single balloon trajectory, for example, may not be representative of bulk

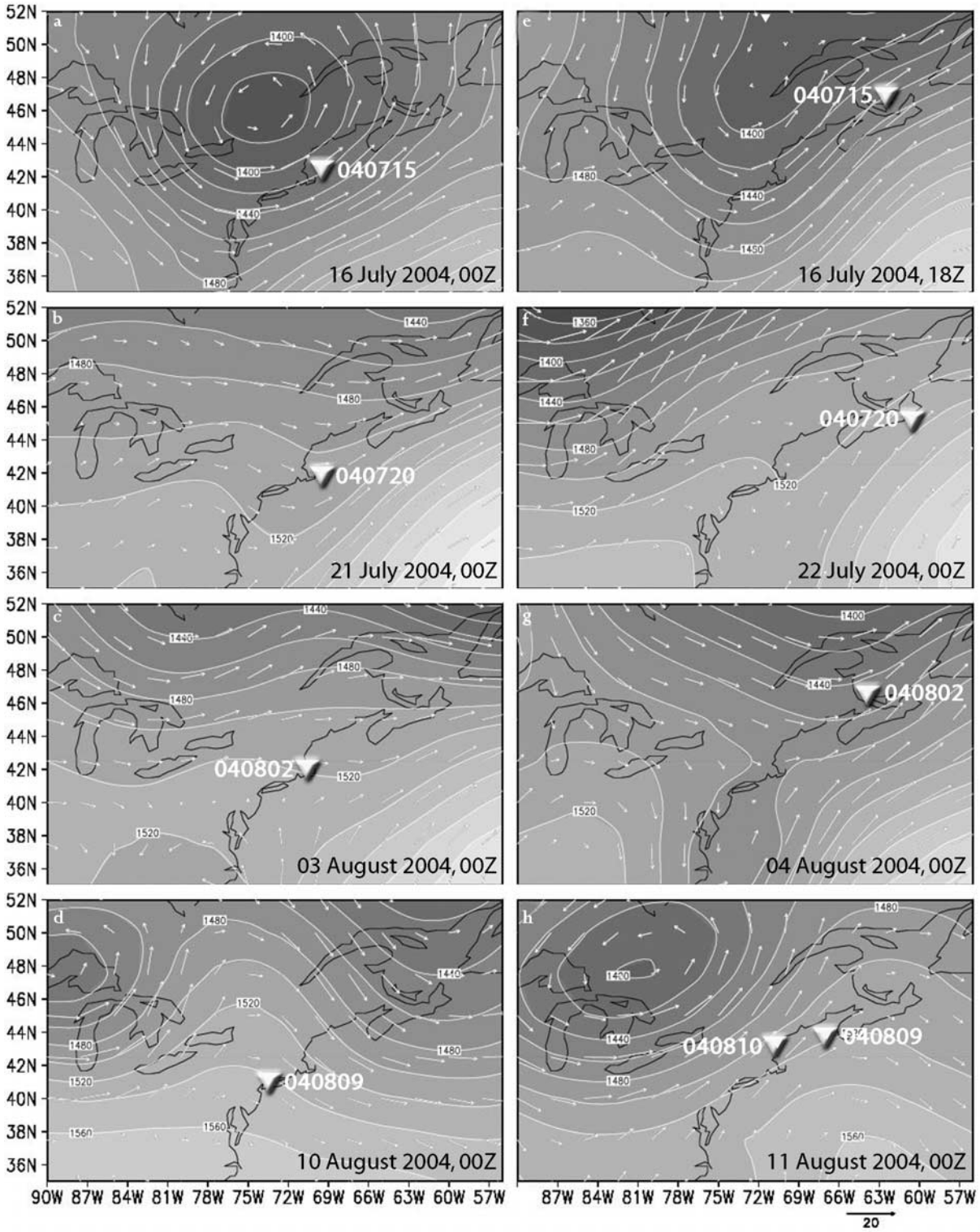

Figure 2. The 850 mbar heights and winds based on 2.5° NCEP II reanalysis data at times spanning the five CMET balloon flights. Balloon locations are indicated with open triangles. While the balloons drifted approximately 1000 m below the 850 mbar level, the wind fields they experienced typically resemble those shown in this figure.

Figure 3. CMET tracking balloon after launch on 2 August 2004.

transport, especially in cases where subgrid-scale flow is important. In addition, because the balloons do not follow vertical air motion, they cannot be used to test errors in the models that result from inaccurate treatment of vertical motion in the atmosphere. This latter limitation may also serve as an advantage, however, because it allows horizontal trajectory errors to be isolated from more complex problem of accurately determining vertical trajectory motion.

[12] While it is useful to understand the statistical accuracy of modeled trajectories, it is also important in the context of ICARTT to be able to pinpoint the actual transport modeling errors associated with individual outflow events. Errors associated with particular model runs can be difficult to predict without an independent means of validation [*Kahl*, 1996]. The five CMET balloons flown during ICARTT were launched into targeted air masses, providing transport model validation during intensive study periods.

3. Balloon Design

[13] Historically, drifting constant volume balloons (CVBs) have been the most commonly used balloons for air mass tracking [e.g., *Angell and Pack*, 1960; *Angell et al.*, 1972]. CVBs have an inextensible shell and therefore float on a constant density surface (approximately a constant altitude). Unfortunately, these simple balloons cannot change altitude during flight or survive additional mass loading due to condensation, particularly at low altitudes. Furthermore, they exhibit a systematic altitude bias between day and night because of the nighttime formation of dew on the balloon envelope.

[14] Air ballasted CVBs overcome these limitations by adding an internal air bladder for reversible buoyancy control. Air ballasted "smart balloons" were first used for air mass tracking during the first and second Aerosol Characterization Experiments (ACE-1 and ACE-2) in 1995 and 1997 [*Businger et al.*, 1999; *R. Johnson et al.*, 2000]. Four "smart balloons" were also flown during ICARTT [*Mao et al.*, 2006; *Businger et al.*, 2006; R. Talbot et al., Smart balloon observations over the North Atlantic: 1. Mini-O3 sampling of urban plumes, unpublished manuscript, 2006].

[15] The Controlled Meteorological (CMET) balloons used in this study (Figure 3) are different from CVBs and smart balloons in that the outer balloon envelope is constructed out of a flexible material, allowing the total balloon volume to change with altitude. This reduces the balloon cost and weight, but also decreases the natural stability that keeps a CVB at a constant altitude. To compensate for this inherent instability, an active buoyancy control algorithm is needed to keep the CMET balloons aloft and permit efficient maneuverability across different levels of the atmosphere.

[16] The CMET balloon buoyancy control system is shown in Figure 4. A flexible outer envelope, with a capacity of 2 m^3, is filled with helium and connected to a rigid 280 liter "superpressure" vessel via a gas transfer device (i.e., a valve and a pump). To increase the balloon buoyancy, lift gas is released from the superpressure vessel into the zero-pressure envelope. To decrease the buoyancy, the flow is reversed. The rigid superpressure vessel can be much smaller than for a CVB because it need only contain a fraction of the lift gas. *Voss et al.* [2005] give a complete discussion of the CMET buoyancy control system and compare it with other altitude control methods.

[17] The balloon payload flown during ICARTT included a two-way satellite modem, a GPS tracking system, a shielded and aspirated temperature sensor, a pressure transducer and, for one flight, relative humidity and ozone instruments. The ICARTT balloons were designed to reach a maximum altitude of 3000 m, though the technology is scalable to higher altitude. The balloons were approximately 1.5 m in diameter when fully inflated and had a total mass of 1.2 kg. Because of their small size and flexible envelope, the CMET balloons could be transported fully inflated in a

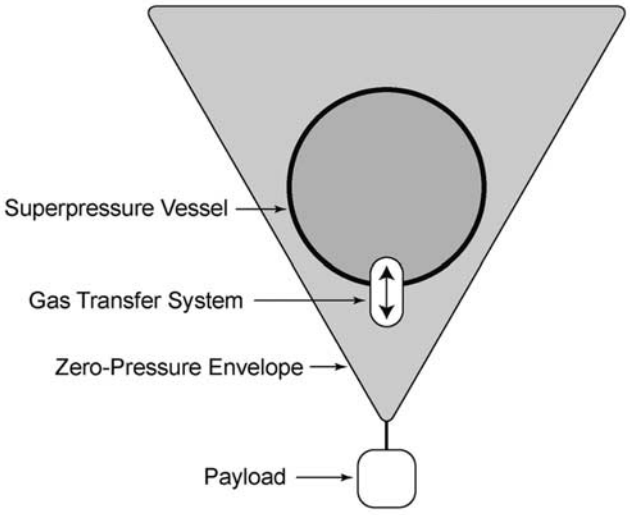

Figure 4. CMET balloon altitude control system [from *Voss et al.*, 2005].

minivan and launched at short notice into targeted pollution events throughout New England.

[18] During ICARTT, buoyancy control was used primarily to maintain a constant altitude in the presence of solar heating of the balloon envelope. It was also used occasionally to avoid topography or restricted air space and, on 11 and 12 August 2004, to perform three successive quasi-Lagrangian soundings of the atmosphere. The relatively low cost of the CMET balloons permits them to be flown as ensembles to observe spatial variations in the wind fields and follow pollution layers at different altitudes. While the ICARTT balloons were generally flown individually and at constant altitude, more recent experiments in both Houston and Mexico City have demonstrated the success of paired balloon flights and continuous soundings to measure atmospheric stability and vertical wind shear during transport (manuscripts in preparation).

4. Trajectory Definition and Computation

[19] An atmospheric "trajectory" is the path taken by an idealized "parcel" of air, given the air parcel's starting location (in space and time) and a time-varying three-dimensional flow field. Assuming an ideal, infinitely small air parcel, the trajectory can be defined by the differential trajectory equation:

$$\frac{\overrightarrow{dX}}{dt} = \overrightarrow{V}\left(\overrightarrow{X}(t), t\right) \tag{1}$$

where $\boldsymbol{X}$ is the vector position of the air parcel, and $\boldsymbol{V}$ is the vector velocity of the flow field at the position of the parcel. Using this equation, once an idealized air parcel is uniquely identified, the path of the parcel is completely defined for all subsequent and prior points in time, allowing unique forward and backward trajectories to be calculated.

[20] An actual air parcel of finite extent can become blurred by turbulent diffusion and sheared by gradients in the wind field. Over short periods of time, however, air parcels remain well enough intact that the parcel centroid remains largely representative of the parcel motion [*Stohl*, 1998]. The length of time over which the concept of an air parcel is valid depends on the stability of the atmosphere, the synoptic conditions and the size of parcel being studied. One of the challenges of using trajectory models is determining how long the trajectory remains representative of bulk transport.

[21] As long as an air parcel remains intact, the mean wind vector field, $|\boldsymbol{V}|$, (averaged over the finite volume of the parcel) should be used in the trajectory equation. Typical numerical model output does not, strictly speaking, provide spatially averaged winds, but rather provides wind speeds at specific points in space (i.e., the interfaces between grid cells) calculated using grid cell averaged thermodynamic variables. Nonetheless, wind fields obtained from current global analyses provide wind information generally representative of large volumes of air, having a typical spatial resolution of 0.3–2°.

[22] The trajectory equation (1) can be solved analytically in only the most idealized flow conditions. Therefore, in the atmosphere, a discrete numerical integration scheme is necessary. The *Pettersen* [1940] integration scheme is commonly used by trajectory models. At any given time, t_i, the parcel position, $\boldsymbol{X}_i$ can be calculated from previous position using the constant acceleration approximation:

$$\overrightarrow{X_i} \approx \overrightarrow{X_{i-1}} + \frac{1}{2}(\Delta t)\left[\overrightarrow{V}\left(\overrightarrow{X_{i-1}}, t_{i-1}\right) + \overrightarrow{V}\left(\overrightarrow{X_i}, t_i\right)\right] \tag{2}$$

where Δt is the size of the time step. $\boldsymbol{X_i}$, can be determined using an iterative procedure [e.g., *Pettersen*, 1940; *Seibert*, 1993; *Stohl*, 1998]. As long as Δt is kept sufficiently small, this integration method will closely approximate the continuous solution to the trajectory equation [*Seibert*, 1993]. Since the velocity field is available only at discrete intervals in time and space, interpolated velocity values are usually used in equation (2), introducing a potentially significant source of error, particularly in rapidly varying conditions.

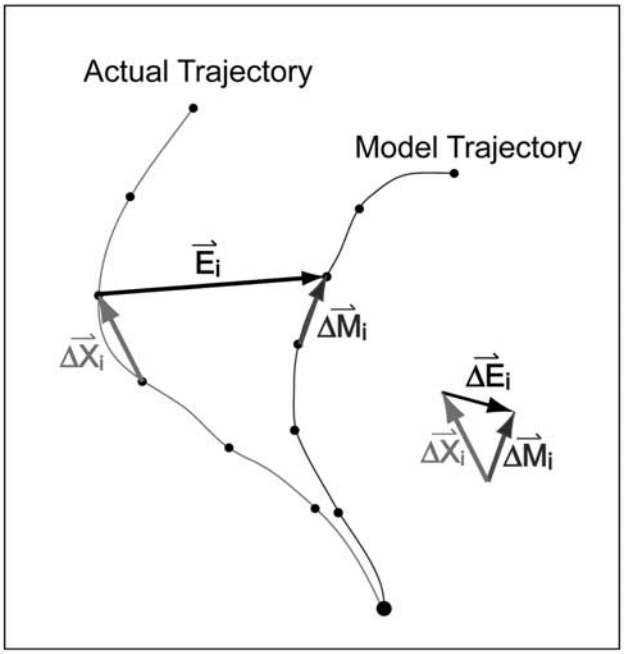

Figure 5. Diagram showing the relationship between the incremental and total trajectory errors at a given iteration of the trajectory equation. The total trajectory error vector, $\boldsymbol{E_i}$, is the vector displacement between the real and model trajectories at a given point in time. The incremental error, $\boldsymbol{\Delta E_i}$, is the vector difference between the real and modeled trajectory displacement vectors for a single iteration.

5. Sources of Trajectory Error

[23] An examination of the trajectory computation equation (2) reveals the origin of trajectory errors. For each iteration of equation (2), the trajectory model will predict a position displacement that is slightly different from the centroid displacement of the real air parcel. This incremental position error, $\boldsymbol{\Delta E_i}$, is the vector difference between the modeled and real trajectory displacement vectors (Figure 5) for a single iteration. After i iterations, the cumulative error,

$\boldsymbol{E}_i$, can be calculated by taking the vector sum of the incremental errors:

$$\overrightarrow{E_i} = \sum_{n=1}^{i} \overrightarrow{\Delta E_n} \tag{3}$$

Thus the cumulative trajectory error depends not only on the magnitude of the incremental errors but on the persistence of their direction.

[24] The cumulative error will be zero at the beginning of the model trajectory and then will tend to grow over time. In the literature, the cumulative position error is often referred to as the absolute horizontal transport deviation (AHTD). The relative horizontal transport deviation (RHTD) is the AHTD divided by the length of the trajectory.

[25] The incremental position error that accumulates at each iteration ($\boldsymbol{\Delta E}_i$ in equation (3)) originates from three possible sources. Truncation errors result from the discrete integration of the trajectory equation. As long as the iteration time step is sufficiently small, the truncation error will be negligible compared with other sources of error. Wind field errors arise from errors in the wind velocity field, $\boldsymbol{V}(\boldsymbol{X}(t))$, used to calculate the trajectory. These errors can result either from nonrepresentative wind measurements, errors in the model forecast or analysis, or from uncertainties associated with interpolating the available model or observational data to the trajectory location and time. Wind field errors are likely to be smaller in regions where the flow field is uniform and larger in regions with large gradients in the wind field.

[26] Finally, wind gradient errors can be introduced during an iteration of equation (2) if the wind field is evaluated at the wrong position. This would occur if the position of the parcel was not well known. Unlike the other sources of error, the magnitude of the incremental wind gradient error is expected to increase with time as the parcel position becomes more and more uncertain. Over horizontal distances of a few hundred kilometers, the wind gradient error is generally smaller than the absolute wind field error. On the other hand, uncertainty in the vertical position of the parcel may lead to large wind gradient errors when vertical wind shear is strong.

6. Model Runs

[27] The FLEXTRA trajectory model [*Stohl et al.*, 1995] is the focus of the present validation study. FLEXTRA is widely used for trajectory modeling applications and its extension for dispersion modeling (FLEXPART) was central to ICARTT mission planning as well as postcampaign analysis [*Stohl et al.*, 2004]. For this study, three-dimensional time-varying wind fields were taken from two sources: (1) the Global Forecast System (GFS) model (1° resolution) and (2) the European Center for Medium-range Weather Forecasts (ECMWF) model using both low (T319) and high (T511) spectral resolution, projected on a 1° and 0.36° grid, respectively. Since analyzed GFS and ECMWF wind fields are available only every 6 hours, 3-hour forecast data were combined with the analyzed data to generate a 3-hour grid. The gridded data were interpolated using bicubic horizontal interpolation, polynomial vertical interpolation and linear temporal interpolation schemes [*Stohl et al.*, 1995].

[28] For each of the five balloon flights, FLEXTRA model trajectories were calculated using the 1° and 0.36° ECMWF and 1° GFS wind fields. The starting latitude and longitude of the modeled trajectories were initialized to the balloons' launch locations. Because of the balloon's non-neutral buoyancy, the vertical trajectory position was fixed through out the flight to the balloon altitude time series, eliminating any vertical position (vertical wind gradient) error. Five-minute position data from the balloon and model trajectories are provided as auxiliary material to this paper.[1]

[29] In order to increase the validation statistics, an additional thirteen nonoverlapping 12-hour flight segments were chosen from the complete set of balloon flight data. Because these segments occurred at separate times, each of them could be treated as an individual quasi-independent balloon flight for trajectory validation purposes. FLEXTRA trajectories initialized at the start of each of these segments were calculated in the same way as for the five complete balloon flights. It should be noted that eight out of these thirteen 12-hour trajectories were taken from different segments of the same flight (040809). While this could potentially bias the results, the flight segments were sufficiently removed in space and time that both the synoptic environment and the skill of the modeled trajectories varied appreciably from the start of one segment to the next. The larger data set of 12-hour trajectories enables statistical analysis of the model trajectory errors. More generally, this trajectory-parsing technique can be used to improve validation results in cases when a small number of long-duration reference trajectories are available.

7. Results

[30] Balloon and model trajectories for the five flights are shown in the first column of Figure 6. For all five flights, the trajectory altitude was approximately 500 m. Trajectories based on high-resolution (0.36°) wind fields do not appear on the plot, but are very similar to the 1.0° ECMWF trajectories. Relative trajectory errors, calculated as a percentage of the balloon trajectory length, are plotted vs. time in the second column of Figure 6. Figure 7 shows complete balloon and model trajectories for flight 040809 which lasted a total of 111 hours and was truncated after 36 hours in Figure 6. Relative and absolute trajectory errors for each model run are summarized in Table 1.

[31] Several notable observations can be made from these data. First, both GFS and ECMWF models underestimated the local wind speeds during all five flights (Figure 6), though the discrepancy was small for all but flight 040720. Both models captured wind directions quite accurately, however, with the exception of the second half of flight 040809 (discussed below). The along-stream trajectory errors were therefore much greater than the cross-stream errors. Since most tracer plumes are generated from a quasi-continuous source and elongated in the along-stream direction [e.g., *Methven and Hoskins*, 1999], along-stream errors will have less of an effect on tracer concentration than cross-

[1] Auxiliary materials are available at ftp://ftp.agu.org/apend/jd/2006jd007456.

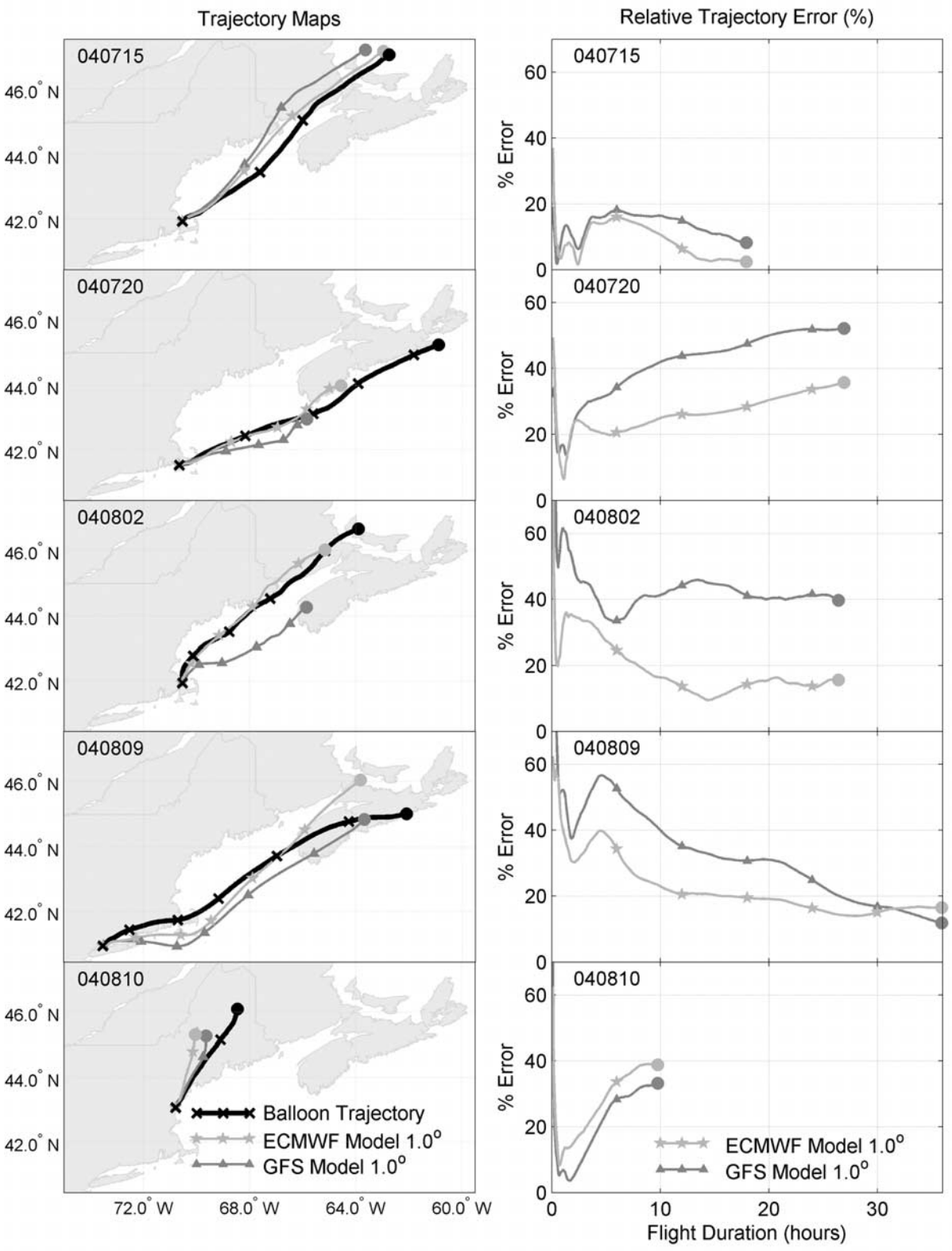

Figure 6. (left) Maps of CMET balloon and FLEXTRA model trajectories and (right) plots showing the time evolution of RHTD errors for each of the five balloon flights. Markers are placed at 6-hour intervals along the trajectories. The trajectories for the 9 August flight are truncated after 36 hours to facilitate comparison. The full trajectories for this flight are plotted in Figure 7.

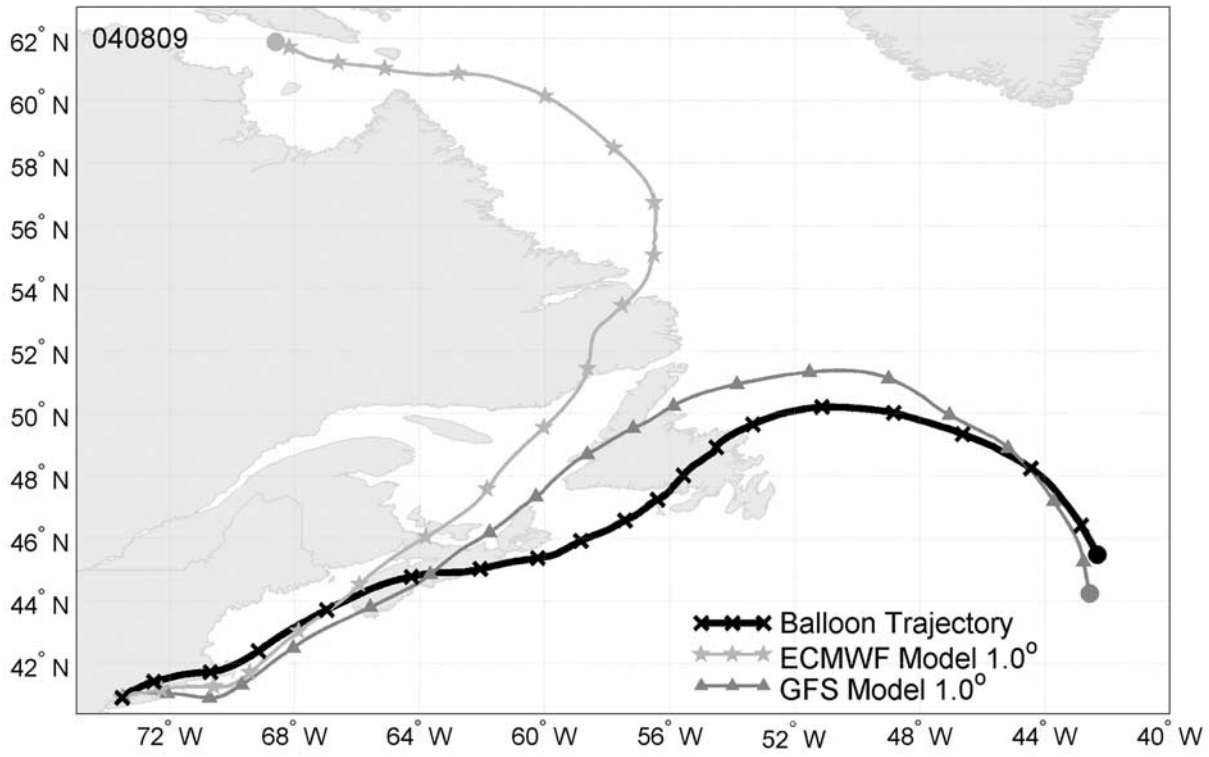

Figure 7. CMET balloon and model trajectories for the flight beginning on 9 August 2004. The ECMWF and GFS model trajectories diverge after 36 hours as the result of a cold front passage.

stream errors. Thus tracer chemistry transport models using the same wind fields may still show significant skill in predicting the position of urban plumes, despite errors in the transport speed of these plumes.

[32] Second, trajectories computed with the ECMWF wind fields were generally more accurate than those computed with GFS output, at least for trajectories shorter than 30 hours in duration. In this time frame, ECMWF trajectory errors were consistently smaller than GFS errors for four out of the five flights, at times by as much as 20%. For the later part of flight 040809, the ECMWF trajectory diverged dramatically from the balloon flight path, while the GFS trajectory remained on course. However, given the larger GFS trajectory error early in the flight, the accuracy of the GFS trajectory may have been a coincidental result of several compensating sources of error. With only one long (30 + hour) flight, it is difficult to assess the long-range accuracy of ECMWF and GFS trajectories from these data. Trajectories computed with the higher-resolution (0.36°) ECMWF data offered only slight improvement over those calculated with the lower-resolution (1.0°) ECMWF data, which is likely related to the fact that the 0.36° resolution approaches the intrinsic maximum spectral resolution of the ECMWF model.

[33] The relative trajectory errors were generally on the high end of those previously reported in the literature. For trajectories based on GFS data, relative errors exceeded the range of previously reported values (10–30%) for three out of the five flights (040720, 040802 and 040810). ECMWF errors also exceeded this range for two of the same flights (040720 and 040810) and grew to more than 80% for the 111-hour flight (040809). The particularly large errors for

Table 1. Summary of Errors for Five ICARTT Flights and a Set of Thirteen 12-Hour Trajectories[a]

			AHTD, km			RHTD, % (min%–max%)		
				ECMWF			ECMWF	
Flight	Duration, hours	Comments	GFS	1.0°	0.36°	GFS	1.0°	0.36°
040715	18	. . .	70	20	20	8 (6–18)	2 (1–16)	2 (1–15)
040720	27	low-level jet	471	323	291	52 (24–52)	36 (20–36)	32 (17–32)
040802	26.5	. . .	306	120	79	40 (33–49)	16 (10–35)	10 (6–32)
040809	111	diffluent flow	139	2482	2370	5 (4–57)	83 (14–83)	79 (14–79)
040810	9.8	approaching cold front	128	150	174	33 (5–33)	39 (15–39)	45 (20–45)
12-hour statistics	12	average of 13 trajectories	108	76	74	33 (33–34)	24 (24–28)	23 (23–27)

[a]In addition to final RHTD and AHTD values, the range of RHTD values in all but the first 2 hours of flight is also reported. The first 2 hours were ignored because relative errors tend to be large initially when trajectory lengths are short.

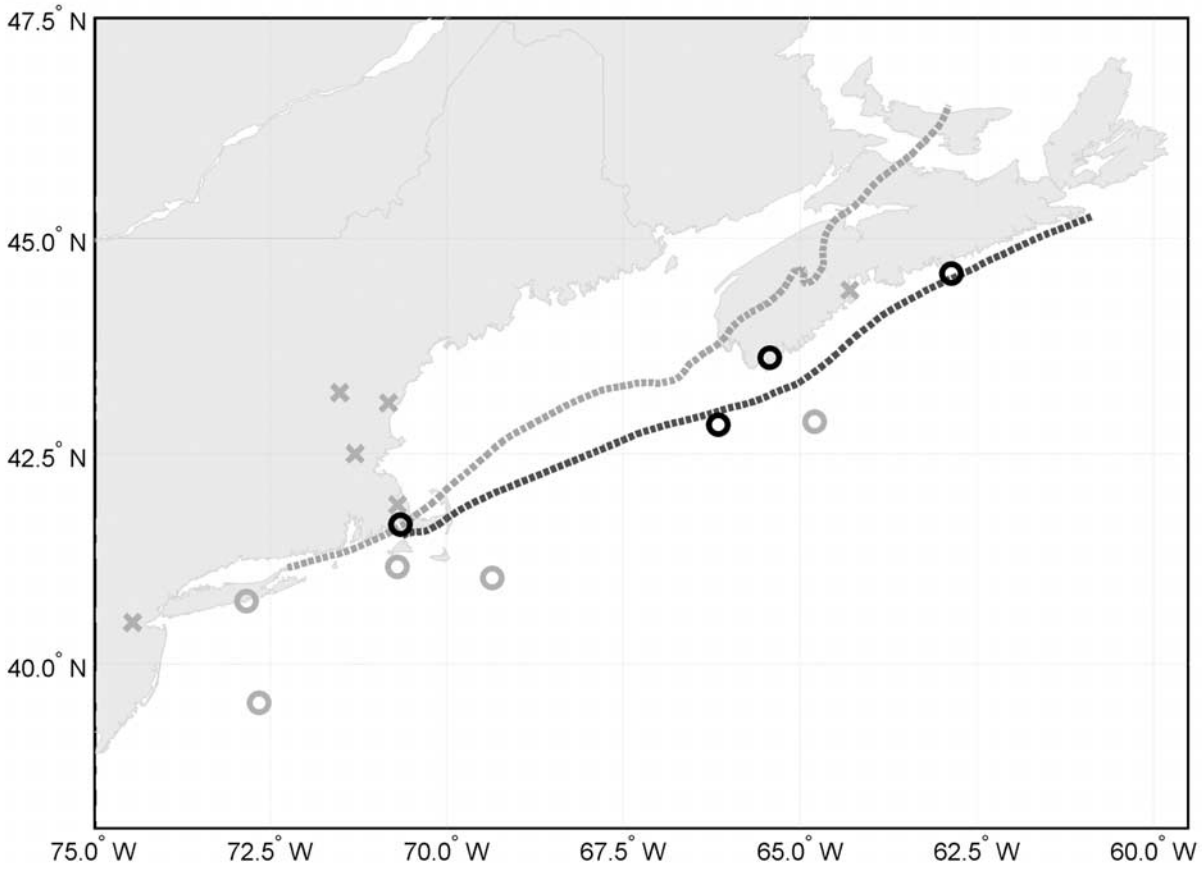

Figure 8. Flight track of CMET balloon 040720 (dotted dark shaded line) and the NOAA smart balloon (dotted light shaded line), with nearby wind profiler stations (crosses) and NOAA P3 aircraft vertical transect locations (circles) from 20 and 21 July 2004. Solid symbols indicate the presence of a low-level jet in the wind observations, while light shaded symbols indicate its absence. Corresponding vertical wind speed profiles are shown in Figure 9. Horizontal P3 transects at approximately 500 m (not shown) also observed the narrow jet off the coast of Nova Scotia. These observations bound the horizontal and vertical dimensions of the jet.

flights 040720, 040809 and 040810 are related to the synoptic and mesoscale flow regimes as discussed below.

7.1. CMET Flight 040720

[34] On 20 and 21 July, CMET balloon 040720 traveled across the Gulf of Maine and along the coast of Nova Scotia at a velocity 1.5 to 2 times as fast as ECMWF and GFS winds predicted. In addition, the balloon traveled 1.5 to 2 times as fast as a NOAA smart balloon that was drifting at a similar altitude only 50–100 km closer to shore [*Businger et al.*, 2006]. At the time of launch, the CMET balloon was only 10 km (and 50 min) away from the passing smart balloon. After drifting for 30 additional hours at nearly identical altitudes, the two balloons were 400 km apart. While FLEXTRA model trajectories dramatically underpredicted the CMET balloon velocity, model trajectories were in good agreement with the smart balloon track.

[35] An examination of aircraft and wind profiler data from these days suggests that the CMET balloon was caught in a narrow low-level jet that was confined to a shallow altitude band with a wind speed maximum at approximately 500 m. Along the coast of Nova Scotia, the jet was approximately 70 km wide, as observed by vertical NOAA P3 spirals, horizontal P3 transects and a wind profiler network (Figures 8 and 9). In these conditions, the CMET balloon position may not be representative of the large-scale flow and may not be an effective reference trajectory. However, given that the balloon was launched into the New York pollution plume, it is evident in this case that plume transport was affected by the low-level jet.

[36] Previous studies have suggested that low-level jets may play a role in rapidly transporting pollutants from US coastal cities up into Maine and eastern Canada [*Fast and Berkowitz*, 1996; *Angevine et al.*, 1996]. Pollutants transported by such coastal jets can be brought onshore in downwind regions by sea breeze recirculation. Because the jet was so narrow and was located just offshore, it was not observed by the network of onshore wind profilers or resolved in any modeled wind fields. To our knowledge, this is the first time a coastal jet has been directly tracked throughout the diurnal cycle. The frequency at which these coastal jets occur in the region is currently unknown.

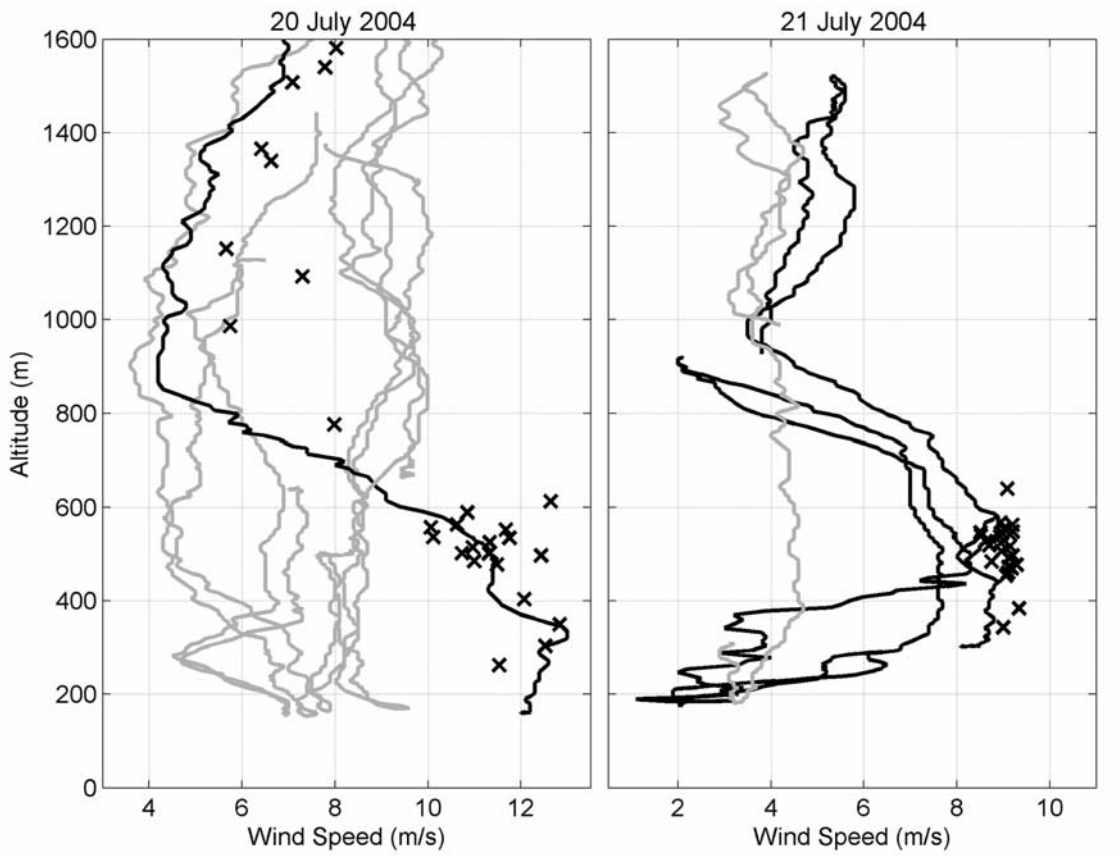

Figure 9. NOAA P3 vertical wind speed profiles (lines) and CMET balloon wind speed measurements (crosses) taken on 20 and 21 July 2004. A low-level wind speed maximum was observed at approximately 400–500 m in some of the P3 profiles (solid lines) and in the CMET balloon data. The baloon trajectory and the P3 sounding locations are shown in Figure 8.

7.2. CMET Flights 040809 and 040810

[37] Large trajectory errors during the final two ICARTT flights can be attributed to the passage of a frontal system through the region on 11 and 12 August. Model trajectories for flight 040809 (the longest flight), remained relatively accurate for the first 36 hours. Midday on 11 August, however, the balloon approached a diffluent region ahead of an approaching front. To the west of the balloon track, the wind field was dominated by a closed cyclonic circulation around a low-pressure system moving in over the Great Lakes region. To the east of the balloon, westerly flow was influenced by anticyclonic circulation around the Azores high (Figure 2h). Because of slight differences in the early positions of the ECMWF and GFS trajectories, the two model trajectories diverged at this point, following the two diffluent airstreams. In these conditions, small errors in either the modeled wind fields or the position of the trajectory can lead to large trajectory errors.

[38] The final balloon (040810) was launched near 0000 UTC on 11 August. At the time of launch an approaching frontal system was creating large horizontal gradients in the wind field. The ETA model showed 850 mbar winds throughout New England differed by more than 10 m/s between Cape Cod and central New York. Under these conditions, model and/or interpolation errors can cause very large errors in the computed trajectories. Previous studies have found that in such complex synoptic environments, an ensemble uncertainty calculation (as provided in the FLEXTRA software) can caution researchers that the modeled trajectories may be inaccurate [e.g., *Merrill et al.*, 1985; *Kahl*, 1993; *Harris et al.*, 2005].

8. Discussion

[39] Previous validation studies have generally reported a single end-of-flight RHTD value for flights ranging from several hours to several days in length. This practice assumes that a linear relationship is maintained between the cumulative trajectory error (AHTD) and the trajectory length. When looking at a single flight, it is difficult to observe such a linear relationship in our data. In Table 1 and Figure 6, it can be seen that RHTD values do not stay constant, but fluctuate by as much as 28% during a single sub-30-hour flight. Since there is nothing unique about the endpoint of a trajectory, such variability makes the reporting of a single RHTD value somewhat arbitrary, particularly when flights of different length are being compared.

[40] In order to investigate this further, we examined the average error taken from the set of thirteen 12-hour trajectories described previously. Figures 10a and 10b show that the average AHTD error does indeed grow linearly with

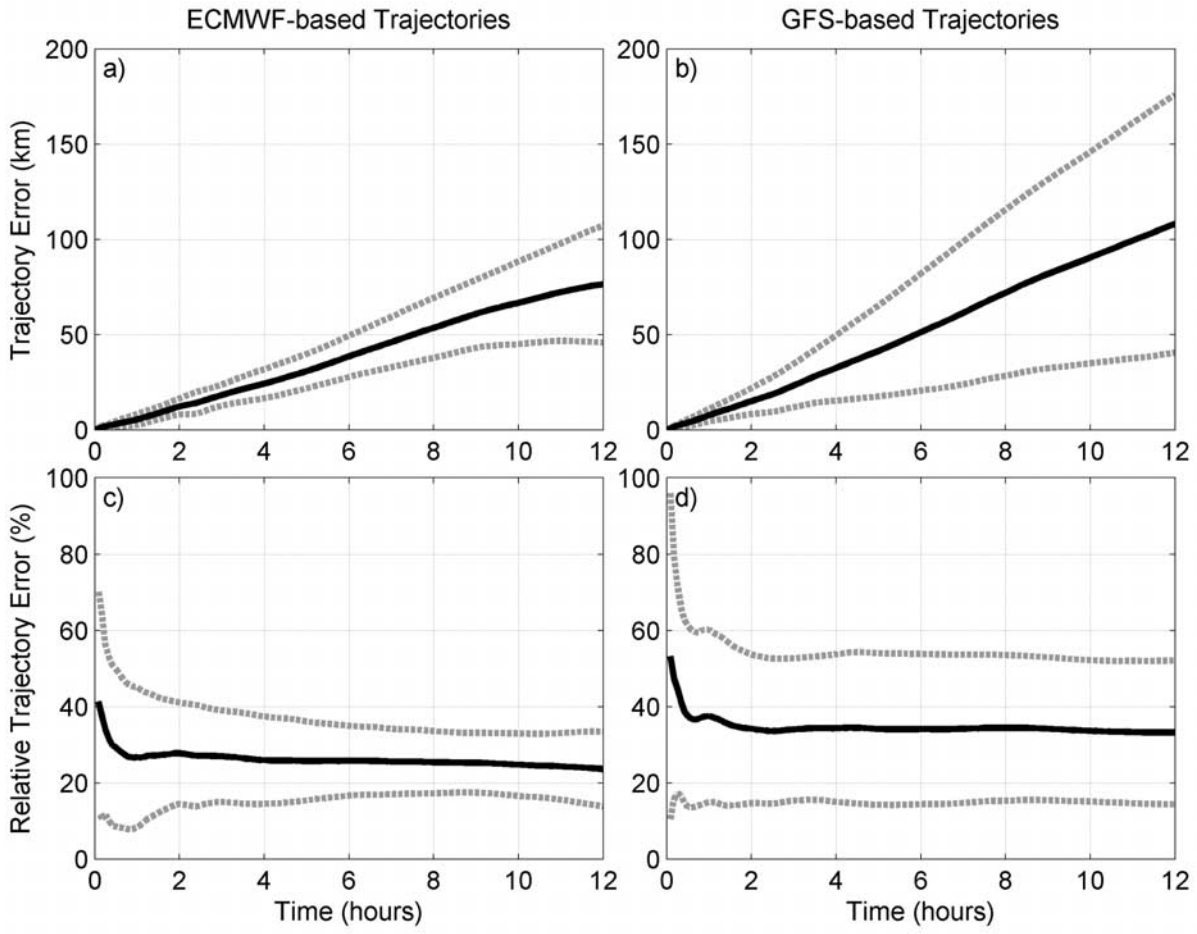

Figure 10. (a and b) Average absolute horizontal transport deviation (AHTD) error and (c and d) average relative horizontal transport deviation (RHTD) error for thirteen 12-hour trajectories based on ECMWF and GFS 1.0° wind fields. A single standard deviation above and below the mean is indicated with dashed shaded lines.

time in both the GFS and the ECMWF models, with a standard deviation approximately 40% of the mean value.

[41] Figures 10c and 10d show the average relative horizontal transport deviation (RHTD) for the set of thirteen trajectories. Considering the variations in the individual trajectory RHTD values, the average RHTD value is surprisingly stable. Between the second and twelfth hour of flight, average ECMWF errors remain within two percentage points of 26% and 25% for resolutions of 1.0° and 0.36° respectively. GFS-based trajectory errors are similarly stable near 34%. Stable RHTD errors were also observed in the average of a smaller set of trajectories for as long as 24 hours. Because of their stability, these average errors are considerably more robust than errors reported at a single point in a single flight.

[42] While often assumed, it is not immediately clear why AHTD errors should be related linearly to the trajectory length. On the contrary, it might be expected that the AHTD errors would increase more rapidly later in the flight as the position of the real air parcel becomes progressively less certain and the wind gradient errors become important. The simple conclusion (that wind gradient errors are simply negligible compared with other errors) also does not appear correct (Figure 11). The solid line in Figure 11 shows the magnitude of the incremental error per unit time step $|\Delta \boldsymbol{E}_i|/\Delta t$ (equation (3) and Figure 5) plotted verses the traveltime. The incremental error (solid line) increases with time, as the distance between real and modeled trajectories grows. This suggests that the wind gradient error is nonnegligible since other sources of error (e.g., truncation and wind field errors) should not show this dependence.

[43] However, because of the nature of the vector sum in equation (3), only the component of $\Delta \boldsymbol{E}_i$ parallel to $\boldsymbol{E}_i$ contributes to the cumulative trajectory error. This component per unit timestep $(\Delta \boldsymbol{E}_i \cdot \boldsymbol{E}_i)/\Delta$t, plotted as the shaded line in Figure 11, does not increase as a function of traveltime. Thus the net effect of the wind gradient error on the AHTD is very small and the average RHTD values remain constant with time.

9. Summary

[44] During ICARTT, five CMET balloons flew a total of 195 flight hours, gathering data on winds and temperature during critical campaign experiments. In two cases, the balloon data helped to guide mission aircraft to targeted urban plumes. This is the first time such small and controllable platforms were used in a research campaign.

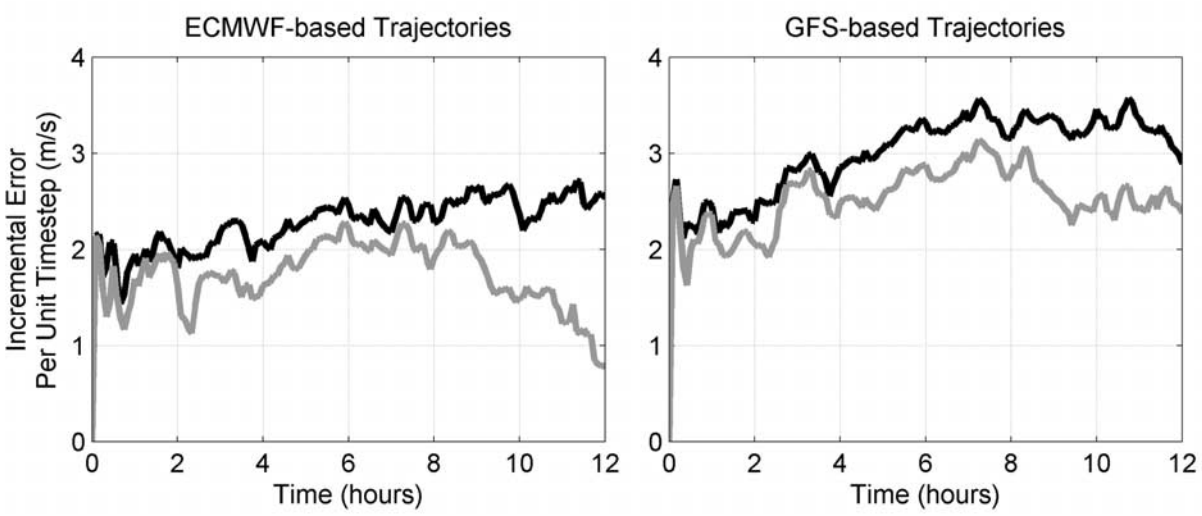

Figure 11. Incremental error per unit timestep ($\Delta \boldsymbol{E_i}/\Delta t$) versus the trajectory traveltime. The solid lines show the total magnitude of the incremental error, while shaded lines show only the component that contributes to the total error growth (($\Delta \boldsymbol{E_i}$ $\boldsymbol{E_i}$)/Δt). Since the cumulative error ($\boldsymbol{E_i}$) increases monotonically with time (Figure 10), the larger traveltimes correspond, on average, with larger absolute separation between the balloon and model trajectories. As in Figure 10, the incremental errors are calculated on the basis of averaging thirteen 12-hour trajectories.

[45] Using a new trajectory-parsing method, data from these flights are compared with output from a trajectory model (FLEXTRA). The parsing technique significantly increased the number of quasi-independent reference trajectories, enabling a more robust statistical treatment of the model errors. For flight segments between 2 and 12 hours, the average RHTD error was found to be 26% of the flight distance when trajectories were based on 1° ECMWF wind fields and 34% of the flight distance when trajectories were based on 1° GFS wind fields. Using higher-resolution wind field data did not significantly improve the trajectories. The errors found here are on the high end of those previously reported in the literature. However, because the errors were generally aligned with the flow direction, the effect on tracer concentrations is likely to be smaller than for cross-stream errors.

[46] Because trajectory errors varied greatly between flights and over the course of a single flight, our results suggest that researchers should try to understand the uncertainties associated with a particular trajectory run. While trajectory errors due to synoptic-scale features may be predictable using ensemble uncertainty calculations [e.g., *Kahl*, 1993], transport due to subgrid-scale features (e.g., a narrow low-level jet) may be missed by both trajectory models and chemical transport models.

[47] The work presented here demonstrates the ability of small controllable balloons to gather high-quality data over multiday flights and support robust statistical analyses. During ICARTT, CMET balloons achieved several important milestones, including targeting urban plumes through rapid deployment, performing repeated soundings on command, and making in situ chemical measurements. These capabilities are being expanded with miniature chemical sensors, flight strategies based on continuous soundings, and the development of propulsion systems for probing the three-dimensional structure of the atmosphere.

[48] **Acknowledgments.** We would like to thank our sponsors, the ICARTT organizers, and the pilots and crew of the NOAA P3 and DC-3 for facilitating this work. We are grateful to Randy Johnson from NOAA ARL/FRD and Steve Businger from the University of Hawaii for providing the 20 July smart balloon trajectory and to the NOAA Earth Systems Research Laboratory for providing wind profiler data. Primary financial support is from the NSF Physical and Dynamic Meteorology Program and NSF Atmospheric Chemistry Program (grant 0137589). Additional support was provided by NOAA (grants NA17RP2632 and NA03OAR4600122) and the Targeted Wind Sensing Program (grant NA04OAR4600157) under the auspices of the AIRMAP program at the University of New Hampshire.

References

Angell, J. K., and D. H. Pack (1960), Analysis of some preliminary low-level constant level balloon (tetroon) flights, *Mon. Weather Rev.*, *88*, 235–248.

Angell, J. K., D. H. Pack, L. Machta, C. R. Dickson, and W. H. Hoecker (1972), Three-dimensional air trajectories determined from tetroon flights in the planetary boundary layer of the Los Angeles basin, *J. Appl. Meteorol.*, *11*, 451–471.

Angevine, W. M., M. Trainer, S. A. McKeen, and C. M. Berkowitz (1996), Mesoscale meteorology of the New England coast, Gulf of Maine, and Nova Scotia: Overview, *J. Geophys. Res.*, *101*, 28,893–28,901.

Baumann, K., and A. Stohl (1997), Validation of a long-range trajectory model using gas balloon tracks from the Gordon Bennett Cup 95, *J. Appl. Meteorol.*, *36*, 711–720.

Businger, S., S. R. Chiswell, W. C. Ulmer, and R. Johnson (1996), Balloons as a Lagrangian measurement platform for atmospheric research, *J. Geophys. Res.*, *101*, 4363–4376.

Businger, S., R. Johnson, J. Katzfey, S. Siems, and Q. Wang (1999), Smart tetroons for Lagrangian air-mass tracking during ACE 1, *J. Geophys. Res.*, *104*, 11,709–11,722.

Businger, S., R. Johnson, and R. Talbot (2006), Scientific insights from four generations of Lagrangian smart balloons in atmospheric research, *Bull. Am. Meteorol. Soc.*, *87*, 1539–1554.

Clarke, J. F., T. L. Clark, J. K. S. Ching, P. L. Haagenson, R. B. Husar, and D. E. Patterson (1983), Assessment of model simulation of long-distance transport, *Atmos. Environ.*, *17*, 2449–2462.

Draxler, R. R. (1987), Sensitivity of a trajectory model to the spatial and temporal resolution of the meteorological data during CAPTEX, *J. Clim. Appl. Meteorol.*, *26*, 1577–1588.

Draxler, R. R. (1991), The accuracy of trajectories during ANATEX calculated using dynamic model analysis versus rawinsonde observations, *J. Appl. Meteorol.*, *30*, 1446–1467.

Draxler, R. R. (1996), Boundary layer isentropic and kinematic trajectories during the August 1993 North Atlantic Regional Experiment Intensive, *J. Geophys. Res.*, *101*, 29,255–29,268.

Fast, J. D., and C. M. Berkowitz (1996), A modeling study of boundary layer processes associated with ozone layers observed during the 1993 North Atlantic Regional Experiment, *J. Geophys. Res.*, *101*, 28,683–28,699.

Feigley, C. E., and H. E. Jeffries (1979), Analysis of processes affecting oxidant and precursors in the Los Angeles Reactive Pollutant Program (LARPP) Operation 33, *Atmos. Environ.*, *13*, 1369–1384.

Haagenson, P. L., Y. H. Kuo, M. Skumanich, and N. L. Seaman (1987), Tracer verification of trajectory models, *J. Clim. Appl. Meteorol.*, *26*, 410–426.

Haagenson, P. L., K. Gao, and Y. H. Kuo (1990), Evaluation of meteorological analyses, simulations, and long-range transport calculations using ANATEX surface tracer data, *J. Appl. Meteorol.*, *29*, 1268–1283.

Harris, J. M., R. R. Draxler, and S. J. Oltmans (2005), Trajectory model sensitivity to differences in input data and vertical transport method, *J. Geophys. Res.*, *110*, D14109, doi:10.1029/2004JD005750.

Johnson, D. W., et al. (2000), An overview of the Lagrangian experiments undertaken during the North Atlantic regional Aerosol Characterization Experiment (ACE-2), *Tellus, Ser. B*, *52*, 290–320.

Johnson, R., S. Businger, and A. Baerman (2000), Lagrangian air mass tracking with smart balloons during ACE-2, *Tellus, Ser. B*, *52*, 321–334.

Kahl, J. D. (1993), A cautionary note on the use of air trajectories in interpreting atmospheric chemistry measurements, *Atmos. Environ., Part A*, *27*, 3037–3038.

Kahl, J. D. W. (1996), On the prediction of trajectory model error, *Atmos. Environ.*, *30*, 2945–2957.

Kahl, J. D., J. M. Harris, G. A. Herbert, and M. P. Olson (1989), Intercomparison of three long-range trajectory models applied to Arctic haze, *Tellus, Ser. B*, *41*, 524–536.

Knudsen, B. M., and G. D. Carver (1994), Accuracy of the isentropic trajectories calculated for the EASOE campaign, *Geophys. Res. Lett.*, *21*, 1199–1202.

Mao, H., R. Talbot, D. Troop, R. Johnson, S. Businger, and A. M. Thompson (2006), Smart balloon observations over the North Atlantic: O_3 data analysis and modeling, *J. Geophys. Res.*, *111*, D23S56, doi:10.1029/2005JD006507.

McQueen, J. T., and R. R. Draxler (1994), Evaluation of model back trajectories of the Kuwait oil fires smoke plume using digital satellite data, *Atmos. Environ.*, *28*, 2159–2174.

Meagher, J. F., L. Stockburger, E. M. Bailey, and O. Huff (1978), The oxidation of sulfur dioxide to sulfate aerosols in the plume of a coal-fired power plant, *Atmos. Environ.*, *12*, 2197–2203.

Merrill, J. T., R. Bleck, and L. Avila (1985), Modeling atmospheric transport to the Marshall Islands, *J. Geophys. Res.*, *90*, 12,927–12,936.

Methven, J., and B. Hoskins (1999), The advection of high-resolution tracers by low-resolution winds, *J. Atmos. Sci.*, *56*, 3262–3285.

Pettersen, S. (1940), *Weather Analysis and Forecasting*, pp. 221–223, McGraw-Hill, New York.

Pickering, K. E., A. M. Thompson, D. P. McNamara, M. R. Schoeberl, H. E. Fuelberg, R. O. Loring Jr., M. V. Watson, K. Fakhruzzaman, and A. S. Bachmeier (1996), TRACE A trajectory intercomparisons: 1. Effects of different input analyses, *J. Geophys. Res.*, *101*, 23,909–23,925.

Reiff, J., G. S. Forbes, F. T. M. Spieksma, and J. J. Reynders (1986), African dust reaching northwestern Europe: A case study to verify trajectory calculations, *J. Clim. Appl. Meteorol.*, *25*, 1543–1567.

Rolph, G. D., and R. R. Draxler (1990), Sensitivity of three-dimensional trajectories to the spatial and temporal densities of the wind field, *J. Appl. Meteorol.*, *29*, 1043–1054.

Seibert, P. (1993), Convergence and accuracy of numerical methods for trajectory calculations, *J. Appl. Meteorol.*, *32*, 558–566.

Stohl, A. (1998), Computation, accuracy and applications of trajectories—A review and bibliography, *Atmos. Environ.*, *32*, 947–966.

Stohl, A., and N. E. Koffi (1998), Evaluation of trajectories calculated from ECMWF data against constant balloon flights during ETEX, *Atmos. Environ.*, *32*, 4151–4156.

Stohl, A., and P. Seibert (1998), Accuracy of trajectories as determined from the conservation of meteorological tracers, *Q. J. R. Meteorol. Soc.*, *124*, 1465–1484.

Stohl, A., G. Wotawa, P. Seibert, and H. Kromp-Kolb (1995), Interpolation errors in wind fields as a function of spatial and temporal resolution and their impact on different types of kinematic trajectories, *J. Appl. Meteorol.*, *34*, 2149–2165.

Stohl, A., O. R. Cooper, R. Damoah, F. C. Fehsenfeld, C. Forster, E.-Y. Hsie, G. Hübler, D. D. Parrish, and M. Trainer (2004), Forecasting for a Lagrangian aircraft campaign, *Atmos. Chem. Phys.*, *4*, 1113–1124.

Stunder, B. J. B. (1996), An assessment of the quality of forecast trajectories, *J. Appl. Meteorol.*, *35*, 1319–1331.

Voss, P. B., E. E. Riddle, and M. S. Smith (2005), Altitude control of long-duration balloons, *J. Aircr.*, *42*, 478–482.

Zak, B. D. (1983), Lagrangian studies of atmospheric pollutant transformations, in *Trace Atmospheric Constituents: Properties, Transformations, Fates*, pp. 303–344, John Wiley, Hoboken, N. J.

D. Holcomb and D. Maczka, Department of Electrical and Computer Engineering, University of Massachusetts, Amherst, MA 01003, USA.

E. E. Riddle, Department of Geosciences, University of Massachusetts, Amherst, MA 01003, USA.

A. Stohl, Norwegian Institute for Air Research, N-2027 Kjeller, Norway.

R. W. Talbot, Institute for the Study of Earth, Oceans, and Space, University of New Hampshire, Durham, NH 03824, USA.

P. B. Voss, Picker Engineering Program, Smith College, Northampton, MA 01063, USA. (pvoss@email.smith.edu)

K. Washburn, Department of Mechanical and Industrial Engineering, University of Massachusetts, Amherst, MA 01003, USA.